JOURNAL OF GUIDANCE, CONTROL, AND DYNAMICS
Vol. 17, No. 6, November–December 1994

Multirate Flutter Suppression System Design for a Model Wing

Gregory S. Mason
Seattle University, Seattle, Washington 98122
and
Martin C. Berg
University of Washington, Seattle, Washington 98195

A new methodology for multirate control system design is described. It accommodates a general multiple-input, multiple-output control law structure that allows the sampling rates for the plant sensor output signals, the update rates for the processor states, and the update rates for the plant control input signals to be independently specified. It includes a capability to design for multiple plant conditions so as to achieve robustness to plant parameter variations. Its analysis components include a method for determining conventional gain and phase margins, a method for determining a bound on the smallest destabilizing uncertainty, and a method for determining the maximum root-mean-square (rms) gain of a multirate system. The methodology is demonstrated by application to the design of a multirate flutter suppression system for a model wing.

Introduction

MULTIRATE control systems occur frequently in engineering practice. They have received comparatively little attention in the technical literature. There are several reasons for this. One is a lack of recognition by the research community of the practical motivations for multirate controllers. Compared to single-rate controllers, they offer the relatively obvious real-time computing efficiencies in multiloop, multifunction, multi-time-scale systems. But with real-time computing hardware costs as low as they are, such efficiencies usually do not justify the additional complexity of a multirate design.

In practice, multirate controllers are often necessitated by hardware constraints. For example, when a sensor provides a signal that is updated only at a fixed interval, except when the update period happens to be a suitable sampling period for a single-rate controller, a multirate controller must be used.

The logistical burden that a multirate system presents is a second reason for the lack of attention given to multirate control systems. This burden is a consequence of the fact that a multirate system is time varying from one sampling instant to the next. Fortunately, a well-designed software package can spare the designer from most of the burden of the logistical difficulties, thereby allowing him or her to concentrate on the more fundamental design issues.

This paper describes a multirate control system design methodology for which we have developed such a software package. The methodology was originally proposed in Ref. 1. It employs the control law synthesis algorithm described in Ref. 2 and the modeling and analysis tools described in Ref. 3 and 4. The description is via an application to the design of a multirate flutter suppression system for a model wing.

The remainder of the paper is divided into four sections. The first describes the model wing, its open-loop characteristics, and the flutter suppression system design goals. The second describes the design methodology and its application to the flutter suppression system design. The third presents the results of the flutter suppression system design. Conclusions are given in the final section.

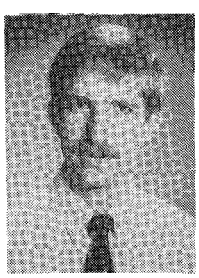

Gregory S. Mason was born in Spokane, Washington, in 1961. He received his M.S. degree in computer integrated manufacturing from the Georgia Institute of Technology in 1984 and his Ph.D. degree in mechanical engineering from the University of Washington in 1992. From 1984 to 1988 he worked in the robotics laboratory at the Naval Undersea Warfare Engineering Station in Keyport, Washington. Currently he is an assistant professor of mechanical engineering at Seattle University. His research interests include digital control, robotics, and flexible automation.

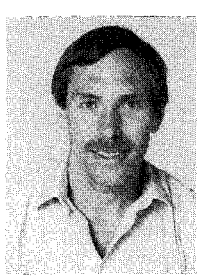

Martin C. Berg was born in Everett, Washington, in 1952. He received his B.S. and M.S. degrees in mechanical engineering from the University of Washington in 1975 and 1978. From 1978 to 1980 he worked in the Flight Controls Research Group for the Boeing Commercial Airplane Company. He entered the Ph.D. program at Stanford University in 1981, where he received his Ph.D. in mechanical engineering in 1986. In 1986 he joined the faculty at the University of Washington, where he is currently an associate professor of mechanical engineering. His research interests involve the design of robust digital control systems, control of flexible electromechanical systems, dynamic system modeling and parameter identification, and multirate digital control.

Received Nov. 5, 1992, revision received Nov. 4, 1993; accepted for publication Nov. 9, 1993.

Problem Description

BACT Wing

The Benchmark Active Controls Technology (BACT) Wing is being developed at the NASA Langley Research Center to study the modeling, prediction, and control of aerodynamic flutter. It consists of a rigid airfoil mounted on a flexible base. The base, called the Pitch and Plunge Apparatus (PAPA), provides the two degrees of freedom necessary to model classical wing flutter. The airfoil has one control surface (CS) located on the trailing edge. Two accelerometers, one near the leading edge (LE) and one near the trailing edge (TE), measure the airfoil's motion. References 5 and 6 describe the BACT Wing in detail.

The flutter suppression system was designed using 16th-order linear state models of the BACT Wing developed by NASA Langley's Structural Dynamics Division. Each model consists of four rigid-body states corresponding to the pitch and plunge modes, six unsteady aerodynamic states, a second-order actuator model, a second-order Dryden filter, and two first-order anti-aliasing filters. Figure 1 shows a block diagram of this structure. NASA provided us with 24 such models, each describing the dynamics of the wing in Freon at a different operating point. The operating points include dynamic pressures above and below the critical flutter pressure at three different Mach numbers. See Table 1 for a summary of the operating points.

Open-Loop Characteristics of the BACT Wing

Two modes, pitch and plunge, dominate the open-loop dynamics of the BACT Wing model. For example, the poles and zeros of the CS command to the LE and TE accelerometer output transfer functions at Mach 0.5 and 75 psf are shown in Figs. 2a and 2b. As dynamic pressure increases, one pair of these poles moves toward the right-half plane and crosses the imaginary axis at the stability boundary. Figure 3 shows this pole movement. The corresponding movements of the open-loop poles not shown in Fig. 3 are relatively small.

The dominant pitch and plunge modes are observable at all operating points with either the TE or the LE accelerometer outputs and are controllable at all operating points using the CS command input. The zeros of the CS command to the TE accelerometer and the CS command to the LE accelerometer transfer functions are shown in Fig. 2 for the Mach 0.5 and 75 psf operating point. As dynamic pressure increases, the non-minimum-phase zeros associated with the TE accelerometer migrate into the left-half plane. The minimum-phase zeros, associated with the LE accelerometer and located near the dominant poles, migrate into the right-half plane. See Fig. 3.

At low dynamic pressures the transfer functions from the CS command input to the TE and LE accelerometer outputs are non–minimum phase. Non–minimum-phase systems are more difficult to control than minimum-phase systems.[7] An alternative output is one that measures the difference between the two accelerometer signals. This new output is essentially pitch acceleration. The CS command to pitch acceleration transfer function is minimum phase for all operating points, and the BACT Wing is relatively easy to control using this new output. We chose not to use this output directly in our designs, however, because it does not adequately account for the inevitable uncertainty in the TE and LE acceleration measurements.

Table 1 Operating points for BACT Wing: Dynamic pressure[a] psf

Mach 0.50	75[b]	100	122	**132**	**150**	**175**	**200**	**225[b]**
Mach 0.70	75	100	125[b]	136	**146**	**175[b]**	**200**	**225**
Mach 0.78	75[b]	100	125	141	**151**	**175**	**200**	**225[b]**

[a]All operating points assume Frean medium. Unstable operating points are boldface.
[b]Operating points used for compensator synthesis.

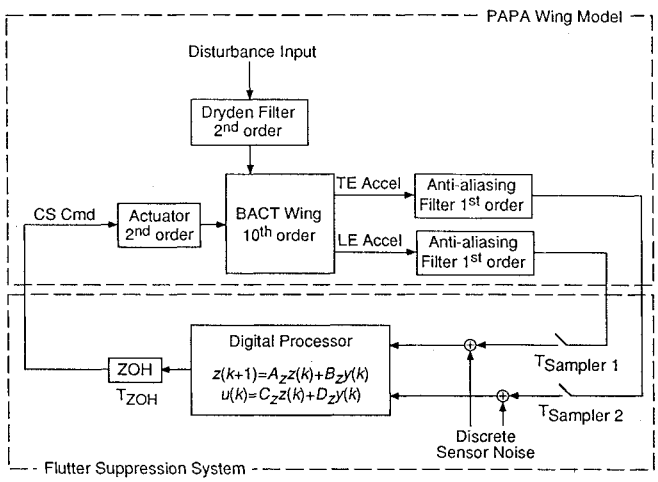

Fig. 1 Block diagram of BACT Wing in feedback with a generic flutter suppression system.

Design Objectives

Our primary objective was to design a multirate flutter suppression system that will stabilize the BACT Wing when it is flown (at some future date) in the wind tunnel at speeds between Mach 0.5 and 0.78 and dynamic pressures between 75 and 225 psf. In addition, the following constraints, most of which are functions of the hardware that will be used to implement the control law, were specified by NASA:

1) *Control activity constraint*: For unity root-mean-square (rms) white-noise input disturbance (1 in./s rms), the steady-state covariance of the CS deflection must not exceed 0.0625 deg^2 (0.25 deg rms), and the CS deflection rate must not exceed 65 deg^2/s^2 (8.0 deg/s rms).

2) *Sampling rate restrictions*: The minimum sampling period is 0.005 s. For multirate sampling, all sampling periods must be multiples of 0.005 s.

3) *Computational delay*: All compensators must account for a minimum 0.005-s computational delay.

4) *Robustness constraints*: The gain and phase margins at the compensator output, which is a scalar signal, must be at least ± 6 dB and ± 45 deg. The maximum singular value of the smallest destabilizing multiplicative uncertainty at the compensator input must be 0.75, which corresponds to simultaneous gain and phase margins at the two sensor inputs to the compensator of ± 6 dB and ± 45 deg.[8]

Finally, our multirate control law was to provide the same performance and stability robustness as a comparable single-rate controller yet require less hardware to implement.

Design Methodology

We designed two flutter suppression systems for the BACT Wing: a single-rate system, for use as a baseline for comparison, and a multirate system. Each was designed using the methodology in Ref. 1. This methodology defines a general approach and provides the specific tools needed to solve a design problem. The methodology has three parts: modeling the multirate system, optimizing the digital processor gains, and analyzing the performance and robustness of the closed-loop system. In the following paragraphs we describe the methodology and its application to the design of the two flutter suppression systems.

Modeling the Flutter Suppression System

A block diagram of a generic flutter suppression system is shown in Fig. 1. In this system, each sampler at the plant output can operate at an independent rate, the digital processor can update each processor state at an independent rate, and each zero-order hold at the compensator output can operate at an independent rate. This compensator model has the form of the generalized multirate control law structure (GMCLS) discussed in Refs. 1, 3, and 4. The GMCLS provides a framework for modeling multirate compensators and eliminates much of the bookkeeping involved with multiple sample/update rates and/or time delays. Using the GMCLS, it is straightforward to represent a multirate system as a periodically time-varying single-rate system. Later we will see that the resulting periodically time-varying system can be further transformed into a time-invariant system by "lifting"[9] or "block processing."[10]

There are two components to the GMCLS: the sampling schedule and the digital processor gains. The sampling schedule indicates the sequence of sample and update activities for all samplers, processor

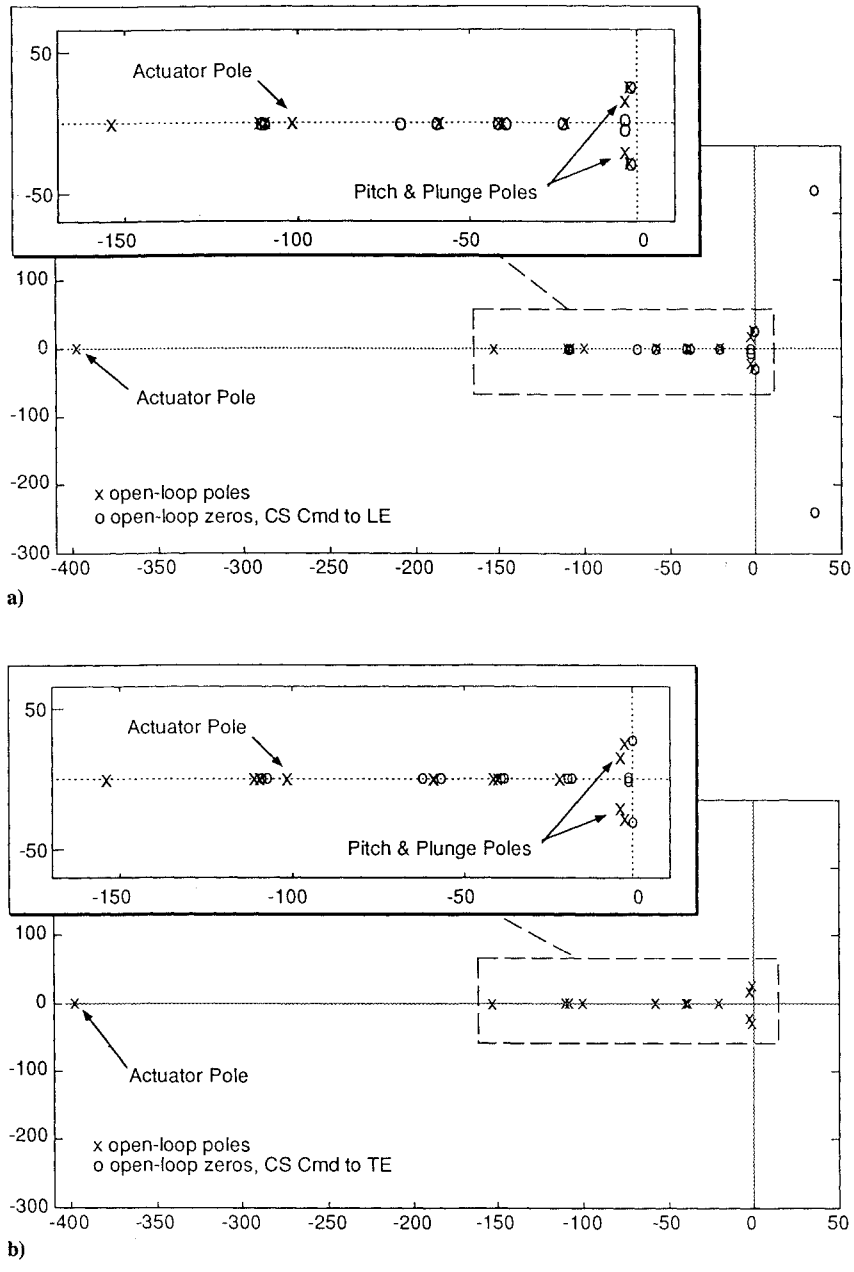

Fig. 2 Open-loop poles and zeros of the CS command to a) LE accelerometer transfer function at Mach 0.50, 75 psf, and b) TE accelerometer transfer function at Mach 0.50, 75 psf.

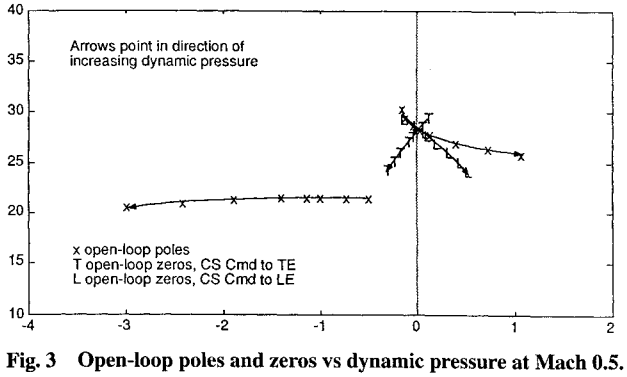

Fig. 3 Open-loop poles and zeros vs dynamic pressure at Mach 0.5.

states, and zero-order holds. In the GMCLS, all sample and update activities must occur at integer multiples of a specified time period T, and the sampling schedule must repeat itself every NT, where N is an integer. Often T and N are functions of the hardware used to implement the control law. The second component of the GMCLS is the digital processor gains A_z, B_z, C_z, and D_z. These gains determine the dynamics of the digital processor and are typically free design parameters.

We modeled both the single-rate and the multirate flutter suppression systems using the framework of the GMCLS. Both compensators have the form of the generic compensator shown in Fig. 1, with two inputs (TE and LE accelerations), one output (CS command), and second-order digital processor dynamics.

The single-rate compensator has a sample/update rate of 50 Hz, which is approximately 10 times the frequency of the dominant pitch and plunge modes. The state-space structure of the compensator's digital processor is

$$\begin{Bmatrix} x_1(n+1) \\ x_2(n+1) \end{Bmatrix} = \begin{bmatrix} 0 & 1 \\ a_1 & a_2 \end{bmatrix} \begin{Bmatrix} x_1(n) \\ x_2(n) \end{Bmatrix} + \begin{bmatrix} 0 & b_1 \\ 1 & b_2 \end{bmatrix} \begin{Bmatrix} \text{TE Accel } (n) \\ \text{LE Accel } (n) \end{Bmatrix} \tag{1a}$$

$$\text{CScmd}(n) = [c_1 \quad c_2] \begin{Bmatrix} x_1(n) \\ x_2(n) \end{Bmatrix} \tag{1b}$$

where x_1 and x_2 are the digital processor states, TE Accel and LE Accel are the acceleration inputs from the analog-to-digital (A/D) converters, and CScmd is the command output to the zero-order hold. Here a_i, b_i, and c_i are the free gains to be optimized. The structure of Eqs. (1) represents a minimal realization of a second-order compensator.[3]

The GMCLS sampling schedule corresponding to the single-rate compensator is shown in Fig. 4. In this figure, circles on each time line indicate when a particular sample or update activity occurs. The GMCLS digital processor gains correspond to the matrix elements in the digital processor's state-space description given in Eqs. (1).

The multirate compensator was designed to provide the same performance and stability robustness as the single-rate compensator using a reduced number of A/D converters. In the multirate compensator, the digital processor states and CS output are updated at 50 Hz, whereas the accelerometers are sampled at 25 Hz. In addition, there is a 0.02-s delay between the sampling of the TE accelerometer output and the LE accelerometer output. Consequently, the multirate compensator requires only one A/D converter to sample both accelerometer outputs.

To maximize the benefits of its multiplexed sampling schedule, the multirate compensator uses periodically time-varying digital processor gains. One set of gains is used when sampling the TE accelerometer output and another set is used when sampling the LE accelerometer output. The state-space structure of the multirate compensator's digital processor is thus

$$\begin{Bmatrix} x_1(n+1) \\ x_2(n+1) \end{Bmatrix} = \begin{bmatrix} 0 & 1 \\ a_1(n) & a_2(n) \end{bmatrix} \begin{Bmatrix} x_1(n) \\ x_2(n) \end{Bmatrix} + \begin{bmatrix} 0 & b_1(n) \\ 1 & b_2(n) \end{bmatrix} \begin{Bmatrix} \text{TE Accel } (n) \\ \text{LE Accel } (n) \end{Bmatrix} \tag{2a}$$

$$\text{CScmd}(n) = [c_1(n) \quad c_2(n)] \begin{Bmatrix} x_1(n) \\ x_2(n) \end{Bmatrix} \tag{2b}$$

where x_1 and x_2 are the digital processor states, TE Accel and LE Accel are the acceleration inputs from the A/D converters, and CScmd is the command output to the zero-order hold. Here $a_i(n)$, $b_i(n)$, and $c_i(n)$ are the free gains to be optimized. These gains are functions of n and are periodically time varying, e.g., $a_i(n) = a_i(n+2)$.

The sampling schedule for the multirate compensator is shown in Fig. 5. Notice the multiplexed sampling scheme of the two A/D converters. The GMCLS digital processor gains correspond to the matrix elements in the digital processor's state-space description given in Eqs. (2), just as in the single-rate case.

Optimizing Digital Processor Gains

To determine the values of the digital processor gains for the two compensators, we used the low-order multirate compensator synthesis algorithm described in Ref. 2, along with the multiple plant conditions idea of Ly.[11,12] The synthesis algorithm uses numerical optimization to determine values of the digital processor gains that minimize a quadratic cost function. The multiple plant conditions idea employs a cost function that is the sum of the costs associated with a single compensator in feedback with a nominal plant and perturbed variations of that plant. The digital processor gains that minimize this new cost function are robust in that they stabilize the nominal plant and the specified variations of that plant.

The multiple plant conditions cost function has the form

$$J_m = \lim_{t\to\infty} \sum_{i=1}^{N_p} E\left\{ \begin{Bmatrix} x_i(t) \\ u_i(t) \end{Bmatrix}^T \begin{bmatrix} Q_i & M_i \\ M_i^T & R_i \end{bmatrix} \begin{Bmatrix} x_i(t) \\ u_i(t) \end{Bmatrix} \right\} \tag{3}$$

where E is the expected-value operator, the integer N_p is the number of simultaneous plant perturbations under consideration; the vectors x_i and u_i represent the plant states and control inputs, respectively, of the ith plant condition; and Q_i, M_i, and R_i are the weighting matrices associated with the ith plant condition and are free parameters selected by the designer.

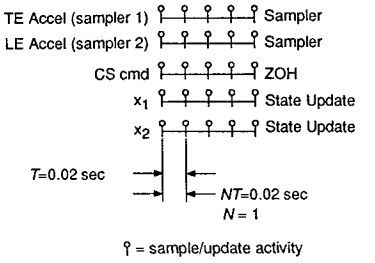

Fig. 4 Sampling schedule for single-rate compensator.

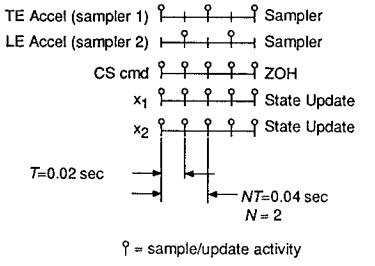

Fig. 5 Sampling schedule for multirate compensator.

Using the synthesis algorithm in Ref. 2 and the cost function in Eq. (3), we found values of the digital processor gains for the single-rate and multirate flutter suppression systems that stabilized the BACT Wing at all 24 operating points. Instead of optimizing over all 24 operating points, however, we selected six representative ones (indicated in Table 1).

For each of the six operating points, we selected a unique set of weights, Q_i, M_i, and R_i, for the cost function in Eq. (3). To select Q_i, M_i, and R_i, we used that fact that the gains that minimize Eq. (3) correspond to the linear quadratic (LQ) regulator feedback gains when the compensator is a continuous-time design, the plant outputs are the values of the plant states, and the compensator is strictly a feedback gain. Accordingly, we first designed a continuous LQ regulator, one for each of the six operating points, that satisfied NASA's performance criterion. The weights were chosen so that the closed-loop damping of the pitch and plunge modes was greater than 0.07, and the rms control surface activity constraints specified by NASA were satisfied. (For comparison, the damping in the open-loop BACT Wing at a stable dynamic pressure of 75 psf is approximately 0.025.) Next, we uniformly scaled Q_i, M_i, and R_i to obtain a unity LQ cost for each operating point for a 6-in./s rms white-noise disturbance input. Finally, we used the values of Q_i, M_i, and R_i from each LQ regulator design for the corresponding values in Eq. (3). Optimum values of the digital processor gains, were found by minimizing the cost function (3) using the synthesis algorithm in Ref. 2.

After optimization, we evaluated each compensator's performance and robustness using the methods discussed in the next section. One of the robustness measures we considered was the maximum singular value of the minimum destabilizing multiplicative uncertainty at the compensator inputs (a structured singular value). The size of the structured singular value for our initial designs was unacceptably small. It was less than 0.20 at some operating points, whereas NASA had specified a value of 0.75. To remedy this we added fictitious sensor noise and reoptimized the processor gains (our initial designs assumed no sensor noise). Our addition of fictitious sensor noise was motivated by the loop transfer recover technique for linear quadratic Gaussian (LQG) systems design.[13]

Analyzing the Flutter Suppression Systems

Recall that we modeled the flutter suppression systems using the GMCLS. It is easy to represent a compensator having the GMCLS as a periodically time-varying single-rate system. Furthermore, it is straightforward to transform a single-rate periodically time-varying system into a single-rate time-invariant system using lifting or block

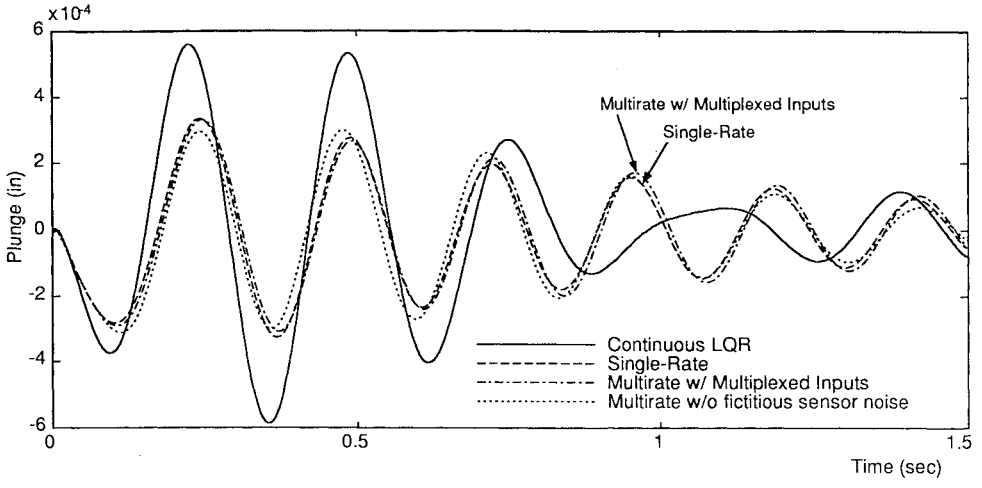

Fig. 6 Closed-loop plunge response to gust pulse disturbance at Mach 0.70, 146 psf.

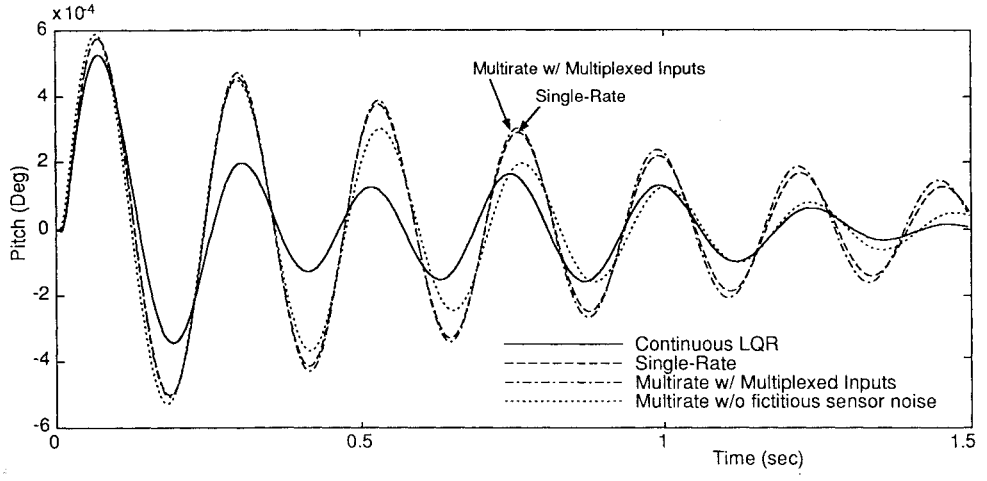

Fig. 7 Closed-loop pitch response to gust pulse disturbance at Mach 0.70, 146 psf.

processing. We refer to the resulting single-rate time-invariant system as the equivalent single-rate system (ESRS). See Refs. 1 or 4 for a discussion of the properties of the ESRS.

An ESRS has the form

$$x(k+N) = A_E x(k) + B_E u_E(k) \tag{4a}$$

$$y_E(k) = C_E x(k) + D_E u_E(k) \tag{4b}$$

where

$$y_E(k) = \begin{Bmatrix} y(k) \\ y(k+1) \\ \vdots \\ y(k+N-1) \end{Bmatrix} \qquad u_E(k) = \begin{Bmatrix} u(k) \\ u(k+1) \\ \vdots \\ u(k+N-1) \end{Bmatrix} \tag{4c}$$

and where the $x(k)$ are the states of the discrete system, $u(k)$ are the discrete inputs, and $y(k)$ are the sampled outputs. The subscript E denotes vectors and matrices strictly associated with the ESRS.

A key feature of an ESRS is that its input/output vectors are composite vectors containing the input/output values of the original system at N sample times. Consequently, an ESRS is always multiple input, multiple output (MIMO) even if the original system is single-input, single output (SISO). Another feature is that an ESRS always has a nonzero direct feedthrough term. When the original system has no dynamics, the direct feedthrough term of its ESRS, D_E, is block diagonal. For example, the ESRS of a constant matrix Δ is, with N blocks,

$$\Delta_E = \text{Block Diag}[\Delta, \Delta, \ldots, \Delta] \tag{5}$$

The ESRS allows one to manipulate and analyze single-rate and multirate systems as if they were both single rate. ESRS state space or corresponding transfer function descriptions can be used to calculate input-output relations for systems in series or in feedback loops just as in classical control.[14] For example, to calculate the ESRS of a time-invariant plant in feedback with a multirate compensator, we would calculate the ESRS of the plant and compensator individually, using the same value of T and N for both, and then combine them using block-diagram algebra. Furthermore, we could determine the stability of the original closed-loop system by calculating the eigenvalues of the new closed-loop ESRS system.[15]

We used the ESRS to evaluate the performance and robustness of our multirate and single-rate flutter suppression systems. First, we formed their closed-loop ESRSs and then we applied analysis techniques for linear time-invariant systems to the resulting single-rate systems. In the following section, we discuss the results of these analyses.

Design Results

By way of review, our two flutter suppression systems are 1) single rate, second order with TE and LE acceleration inputs and CS command output and 2) multirate, second order with multiplexed TE and LE acceleration inputs and CS command output.

We compared the performance and robustness of these two compensators in the following areas: 1) gust pulse response, 2) maximum rms gain from disturbance to the control surface deflection and deflection rate, 3) gain and phase margins at the compensator output, and 4) maximum singular value of the minimum destabilizing multiplicative uncertainty at the compensator input.

The results are presented for three operating points: Mach 0.50, 132 psf: Mach 0.70, 146 psf: and Mach 0.78, 151 psf. Each of these is

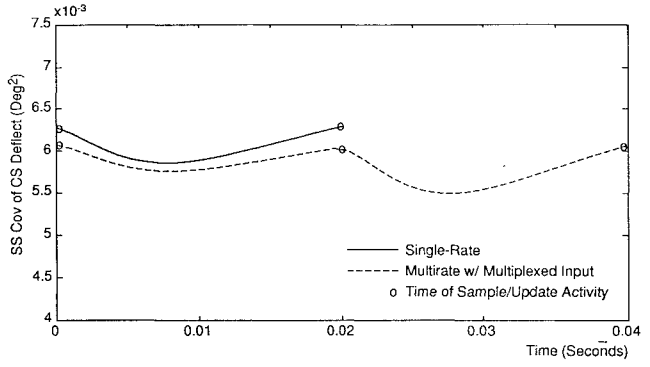

Fig. 8 Propagation of steady-state covariance of CS deflection at Mach 0.70, 146 psf.

5 psf above the critical flutter dynamic pressure for the corresponding Mach number, so the BACT Wing is nominally unstable at each of these operating points. It is important to note that none of these operating points were used for the compensator optimization and so the compensators were not tuned to these particular operating points. Although we will discuss performance and robustness at only three operating points, the following results are indicative of the compensator's performance and robustness at all 24 operating points.

Gust Pulse Response

The gust pulse response provides an indication of the transient response of the closed-loop system to a disturbance input. We computed the gust pulse response by simulating the response of the BACT Wing in feedback with the flutter suppression system to a disturbance input pulse with an amplitude of 10 in./s and a duration of 0.004 s.

Figures 6 and 7 show the response of the BACT Wing at Mach 0.70 and 146 psf to the specified disturbance gust pulse. Also shown is the response of the wing with a continuous LQ regulator. The cost function weights for this LQ regulator design satisfy the same design criterion as were used in the multirate and single-rate designs. The gust pulse responses at the other operating points are similar to those shown in Figs. 6 and 7.

For comparison, gust pulse response plots for the multirate compensator synthesized without fictitious sensor noise are also shown in Figs. 6 and 7. Recall that we added fictitious sensor noise to the multirate design in order to improve the robustness at the compensator input. The primary effect of adding sensor noise is to decrease the damping of the pitch and plunge modes. As can be seen, the reduction in damping is more prevalent in the pitch response than in the plunge response.

Maximum rms Gains

One of NASA's specifications was a limit on the steady-state covariance of the control surface deflection and deflection rate for a 1-in./s rms white-noise disturbance. Our closed-loop system consists of a continuous plant and a discrete compensator. Therefore, these steady-state covariances are periodically time varying. In Fig. 8, we show the steady-state covariance propagation for the BACT Wing in feedback with the two compensators at an operating point of Mach 0.70 and 146 psf for a unity rms white-noise disturbance.

One meaningful interpretation of NASA's specification would be to look at the peak steady-state covariance value taken from the covariance plot. This value, though, is an upper limit on the closed-loop gain for a white-noise disturbance and is not a true indicator of the control activity level. A better measure of control activity would be the maximum rms gain.

The maximum rms gain of a multirate system is given by

$$\sup_{\text{rms}(u)\neq 0} \frac{\text{rms}(y(k))}{\text{rms}(u(k))} = \sup_{\text{rms}(u_E)\neq 0} \frac{\text{rms}(y_E(k))}{\text{rms}(u_E(k))} = \left\| G_E(z^N) \right\|_\infty \quad (6)$$

where $\|G_E(z^N)\|_\infty$ is the H-infinity norm of the transfer function of the ESRS system between the input and output of interest, u and y, respectively. See Refs. 1 and 4 for details.

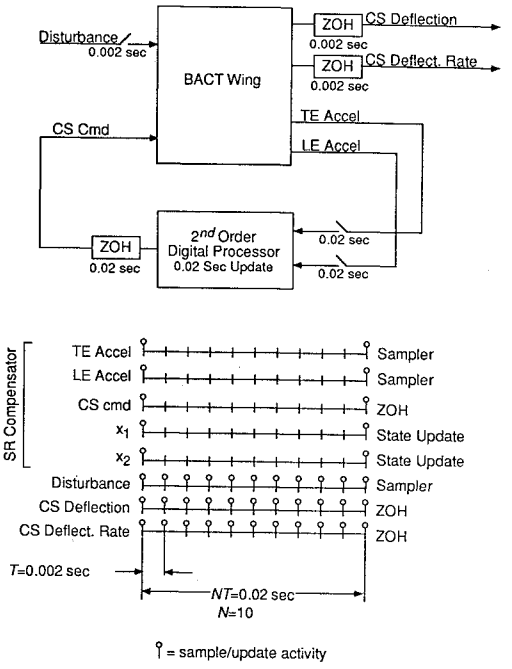

Fig. 9 Block diagram and corresponding sampling schedule for the system used to evaluate the maximum rms gain.

To apply the discrete equation (6) to our mixed continuous/discrete system, we created a new discrete multirate system in which the continuous inputs and outputs of interest are sampled very fast. We chose a sampling rate for the CS deflection and deflection rate of 500 Hz. This is more than 10 times the control surface actuator roll-off frequency. Figure 9 shows a block diagram and sampling schedule of this new discrete-time system in feedback with the single-rate compensator. This closed-loop system is multirate even though the compensator is single rate. The ESRS for the system has a sample/update rate of 500 Hz and an N of 10.

We used this new ESRS system to estimate the maximum rms gain of the original single-rate system between the disturbance and the CS deflection and deflection rate. A similar method was used to calculate the maximum rms gains for the disturbance input to the CS deflection and deflection rate for the multirate flutter suppression system. The results for the BACT Wing at the three representative operating points are summarized in Table 2.

Gain and Phase Margins

Gain and phase margins were calculated at the compensator output using the ESRS and a multiloop Nyquist diagram. The ESRS of the plant and compensator were computed independently and then combined in series to form the ESRS loop transfer function. Gain and phase margins were subsequently measured directly off the multiloop Nyquist plot of this function. These are traditional gain and phase margins and assume that the gain and phase cannot vary simultaneously. The details of this technique are given in Refs. 4 and 16.

The gain and phase margins for the BACT Wing at the three operating points are presented in Table 2. These values are typical of the margins at all 24 operating points, although the margins tend to be better at lower dynamic pressures and slightly worse at higher dynamic pressures. A representative Nyquist diagram is shown in Fig. 10. This particular Nyquist plot has two encirclements of the -1 point because the open-loop plant has two unstable poles.

Robustness at the Compensator Input

The uncertainty at the compensator input was assumed to be a multiplicative perturbation of the form shown in Fig. 11, where k_1 and k_2 are complex gains. We transformed this system into the output feedback form traditionally used in robustness analysis using simple block-diagram algebra. However, when the compensator is multirate, we must use the ESRS of the plant, compensator, and uncertainty. A block diagram of this closed-loop ESRS for the mul-

Table 2 Performance and robustness summary

	Mach 0.50, 132 psf		Mach 0.70, 146 psf		Mach 0.78, 151 psf	
	Single rate	Multirate	Single rate	Multirate	Single rate	Multirate
Maximum rms gain, distribution to CS deflection rate, deg s/in.	0.22	0.25	0.19	0.19	0.11	0.11
Maximum rms gain, distribution to CS deflection rate, deg/in.	6.5	6.9	2.4	2.6	1.5	1.5
Gain margin, dB	12	12	10	10	9	9
Phase margin, deg	41	38	45	40	43	40
$\bar{\sigma}\begin{bmatrix} k_1 & 0 \\ 0 & k_2 \end{bmatrix}$	0.41	0.45	0.38	0.44	0.35	0.45
$\bar{\sigma}\begin{bmatrix} k_1 & 0 \\ 0 & k_2 \end{bmatrix}$ without sensor noise	0.25	0.35	0.26	0.32	0.25	0.31

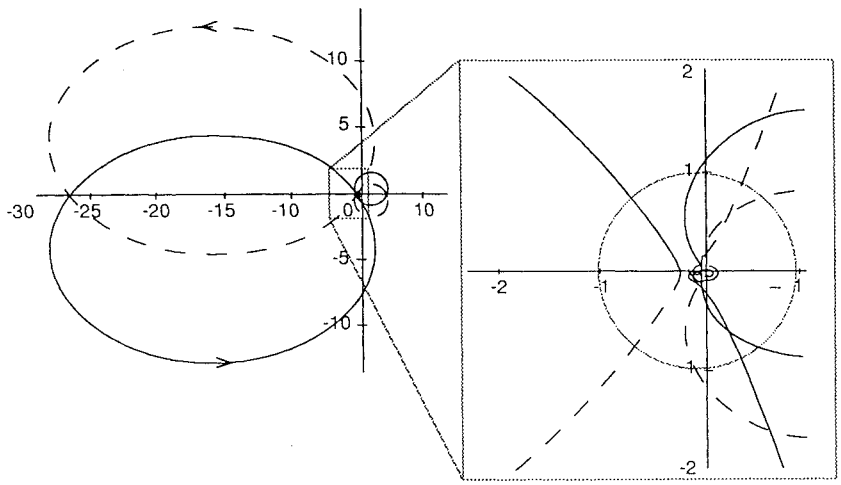

Fig. 10 Nyquist diagram of BACT Wing and multirate compensator at Mach 0.70, 146 psf, with loop broken at compensator output.

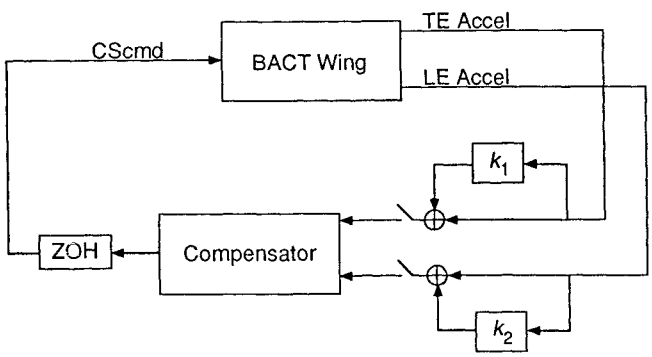

Fig. 11 BACT Wing with uncertainty at compensator input.

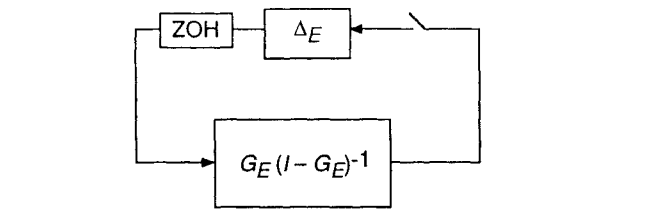

Fig. 12 ESRS for system in Fig. 11.

tirate flutter suppression system is shown in Fig. 12. Here G_E is the loop transfer function comprised of the compensator and plant ESRS transfer functions connected in series.

Now, given the system in the form shown in Fig. 12, we can calculate an exact value for the size of the smallest destabilizing perturbation.[17] First rewrite Δ_E in Fig. 12 as

$$\Delta_E = I_1 k_1 + I_2 k_2 \tag{7}$$

where $I_1 = \text{diag}\{1\ 0\ 1\ 0\ \cdots\ 1\ 0\}$ with $2N$ diagonal elements and where I_2 has a similar form. Then it can be shown that[17]

$$\bar{\sigma}(\Delta_{\min}) = \left(\sup_{\phi} \max_{\theta} \rho\left[\left(I_1 + I_2 e^{j\theta}\right) H_E(e^{j\phi})\right] \right)^{-1} \tag{8}$$

where $\bar{\sigma}(\Delta_{\min})$ represents the maximum magnitude of the smallest destabilizing k_1 or k_2, $0 \le \phi \le \pi$, $0 \le \theta \le 2\pi$, ρ is the spectral radius, and $H_E(z^N) = G_E(z^N)[I - G_E(z^N)]^{-1}$.

We are guaranteed that the system in Fig. 11 will remain stable if

$$\bar{\sigma}\begin{bmatrix} k_1 & 0 \\ 0 & k_2 \end{bmatrix} < \bar{\sigma}(\Delta_{\min}) \tag{9}$$

We are also guaranteed that when inequality (9) is violated, there exist values of k_1 and k_2 that destabilize the system in Fig. 11.

Equation (8) is straightforward to solve with a two-dimensional search in ϕ and θ. The results are given in Table 2. For comparison, the corresponding results for the design without the fictitious sensor noise are also given in Table 2. Notice that the addition of the fictitious noise increases the maximum singular value of the smallest destabilizing uncertainty by as much as 60%.

Even with the fictitious sensor noise, the robustness at the compensator inputs does not meet NASA's specification of a maximum singular value of 0.75. We could have improved the robustness at the compensator output further by increasing the fictitious sensor noise level, but we chose not to do so because doing so simultaneously reduces the gain and phase margins at the compensator output.

Conclusions

A new methodology for multirate control system design has been developed. It accommodates a general multiple-input multiple-output control law structure that allows the sampling rates for the plant sensor output signals, the update rates for the processor states, and the update rates for the plant control input signals to be independently specified. It includes a capability to synthesize a single control law for multiple plant conditions so as to achieve robustness to plant parameter variations. Its analysis components include a method for determining conventional gain and phase margins, a method for determining a bound on the smallest destabilizing uncertainty, and a method for determining the maximum rms gain of a multirate system. As is demonstrated in this paper, by application to the design of a multirate flutter suppression system for a model wing, this new methodology is a practical and effective tool for multirate control system design.

Acknowledgment

This research was supported by NASA Langley Research Grants NAG-1-1055 and NCC1-156.

References

[1]Mason, G. S., "Multirate Compensator Synthesis and Analysis," Ph.D. Dissertation, Univ. of Washington, Seattle, WA, 1992.

[2]Mason, G. S., and Berg, M. C., "Reduced-Order Multirate Compensator Synthesis," *Journal of Guidance, Control, and Dynamics*, Vol. 15, No. 3, 1992, pp. 700–706.

[3]Berg, M. C., Mason, G. S., and Yang, G. S., "A New Multirate Sampled-Data Control Law Structure and Synthesis Algorithm," *Journal of Guidance, Control, and Dynamics*, Vol. 15, No. 5, 1992, pp. 1183–1191.

[4]Mason, G. S., and Berg, M. C., "Robustness Analysis of a Multirate Flutter Suppression System," *Journal of Guidance, Control, and Dynamics*, Vol. 16, No. 5, 1993, pp. 992–926.

[5]Bennett, R. M., Eckstrom, C. V., Rivera, J. A. Jr., Dansberry, B. E., Farmer, M. G., and Durham, M. H., "The Benchmark Aeroelastic Models Program: Description and Highlights of Initial Results," NASA Tech. Memo. 104180, Dec. 1991.

[6]Durham, M. H., Keller, D. F., Bennett, R. M., and Wieseman, C. D., "A Status Report on a Model for Benchmark Active Controls Testing," AIAA Paper 91-1011, April 1991.

[7]Freudenberg, J. S., and Looze, D. P., "Right Half Plane Poles and Zeros and Design Tradeoffs in Feedback Systems," *IEEE Transactions on Automatic Control*, Vol. 30, No. 6, 1985, pp. 555–565.

[8]Mukhopadhyay, V., and Newsom, J. R., "A Multiloop System Statility Margin Study Using Matrix Singular Values," *Journal of Guidance, Control, and Dynamics*, Vol. 7, No. 5, 1984, pp. 582–587.

[9]Meyer, R. A., and Burrus, C. S., "A Unified Analysis of Multirate and Periodically Time-Varying Digital Filters," *IEEE Transactions Circuits in Systems*, Vol. CAS-22, No. 3, 1975, pp. 162–168.

[10]Meyer, D. G., "A New Class of Shift-Varying Operators, Their Shift-Invariant Equivalents, and Multirate Digital Systems," *IEEE Transactions on Automatic Control*, Vol. AC-35, No. 4, 1990, pp. 429–433.

[11]Ly, U. L., "A Design Algorithm for Robust Low-Order Controllers," Ph.D. Dissertation, Stanford Univ., Stanford, CA, 1982.

[12]Ly, U. L., "Robust Control Design Using Nonlinear Constrained Optimization," *Proceedings of the American Control Conference*, IEEE, Piscataway, NJ, 1990, pp. 968, 969.

[13]Doyle, J. C., and Stein, G., "Multivariable Feedback Design: Concepts for a Classical/Modern Synthesis," *IEEE Transactions on Automatic Control*, Vol. AC-26, No. 1, 1981, pp. 4–16.

[14]Khargonekar, P. P., Poolla, K., and Tannenbaum, A., "Robust Control of Linear Time-Invariant Plants Using Periodic Compensators," *IEEE Transactions on Automatic Control*, Vol. AC-30, No. 11, 1985, pp. 1088–1096.

[15]Kono, M., "Eigenvalue assignment in Linear Periodic Discrete-Time Systems," *International Journal of Control*, Vol. 32, No. 1, 1980, pp. 149–158.

[16]Thompson, P. M., "Gain and Phase Margins of Multirate Sampled-Data Feedback Systems," *International Journal of Control*, Vol. 4, No. 3, 1986, pp. 833–846.

[17]Doyle, J., "Analysis of Feedback systems with Structured Uncertainties," *IEEE Proc.*, Vol. 129, Pt. D, No. 6, 1982, pp. 243–250.